Anisotropy of the mobility of pentacene from frustration

Gilles A. de Wijs[a,b,*], Christine C. Mattheus[a], Robert A. de Groot[a,b],
Thomas T.M. Palstra[a]

[a]*Laboratory of Chemical Physics, Materials Science Centre, Nijenborgh 4, NL-9747 AG Groningen, The Netherlands*
[b]*Computational Materials Science, FOM Institute for Condensed Matter, Toernooiveld 1, NL-6525 ED Nijmegen, The Netherlands*

Abstract

The bandstructure of pentacene is calculated using first-principles density functional theory. A large anisotropy of the hole and electron effective masses within the molecular planes is found. The band dispersion of the HOMO and the LUMO is analyzed with the help of a tight-binding (TB) fit. The anisotropy is shown to be intimately related to the herringbone structure.
© 2003 Elsevier Science B.V. All rights reserved.

Keywords: Pentacene; Bandstructure; Effective mass; Anisotropy; Mobility

1. Introduction

Charge transport in organic molecular conductors has gained prominent interest as it is expected that in ultra-clean materials band transport with high electronic mobilities can be obtained. Recent progress in synthetic procedures have minimized mobility reducing factors, such as disorder, Frenkel defects, and Schottky defects. Thus, mobilities up to ∼1 cm^2/(V s) have been obtained in thin film devices and in single crystals at room temperature [1–4].

Pentacene has gained prominent interest because of a number of favorable materials properties. Large single crystals can be easily grown by vapor transport [5], and the material can be handled in air. The reactivity of pentacene to impurity levels of oxygen and hydrogen is often underestimated, but can be minimized using appropriate synthetic conditions [6]. Despite the presence of at least four different polymorphs [7], there are no structural phase transitions observed for the most stable polymorph, the single crystal polymorph [8–10]. The layered crystal structure indicates a highly two-dimensional charge transport.

In this paper, we use first-principles density functional theory (DFT) to calculate the bandstructure of pentacene. We find a very large anisotropy of the effective mass within the layers, resulting from a frustration of the electron transfer along the crystallographic *b*-axis. This frustration is rationalized using a tight-binding (TB) fit of the bandstructure, and

is intimately related to the herringbone geometry of the crystal structure of pentacene. Our results imply that the mobility is strongly directionally dependent within the layers.

2. Structure

The crystal structure of bulk pentacene, depicted in Fig. 1, has been reported by several groups [8–10]. It is a layered structure, triclinic, with spacegroup $P\bar{1}$. The molecular layers consist of pentacene molecules arranged in a herringbone pattern. We chose the unit vectors following [9], with *a* and *b* in the molecular plane and *c* inter-relating the molecular planes. The unit cell contains two inequivalent molecules. The molecules are not perpendicular to the molecular planes, but are at finite angles. This slant can be understood as a relative shift of the molecules. Starting from one molecule, moving along $(\boldsymbol{a} + \boldsymbol{b})/2$ one arrives at an another (inequivalent) molecule, that is shifted along its longest molecular axis (LMA) by 2.13 Å, i.e. approximately the length of one ring in the pentacene molecule. Going along $(\boldsymbol{a} - \boldsymbol{b})/2$ the shift is a mere 0.12 Å, i.e. it is negligible. This "staircase" pattern is indicated in Fig. 1b, which shows a projection of a molecular layer along the LMA.

3. Technical details

The bandstructure has been calculated using density functional theory in the generalized gradient approximation

* Corresponding author. Tel.: +31-24-3651984; fax: +31-24-3652120.
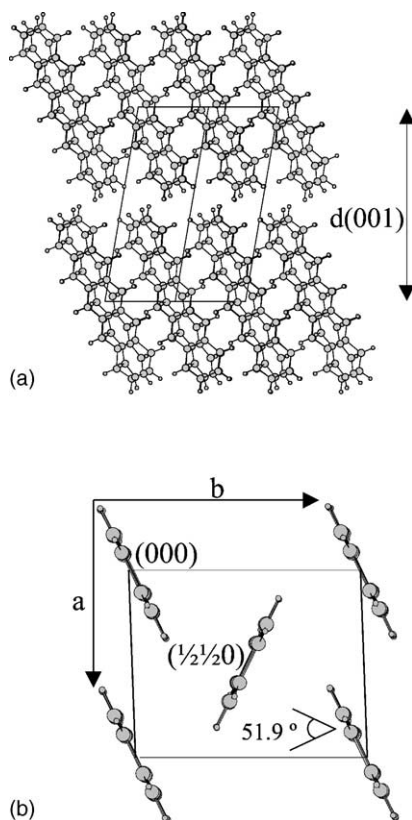*E-mail address:* dewijs@baserv.uci.kun.nl (G.A. de Wijs).

Fig. 1. The crystal structure of pentacene. (a) Stacked layers of pentacene molecules, viewed along the $[1\bar{1}0]$-axis. A unit cell is also indicated. (b) Projection of the pentacene crystal structure and its unit cell vectors *a* and *b* on a plane perpendicular to the long molecular axes (LMA). The angle between the molecules is indicated. The herringbone arrangement is evident.
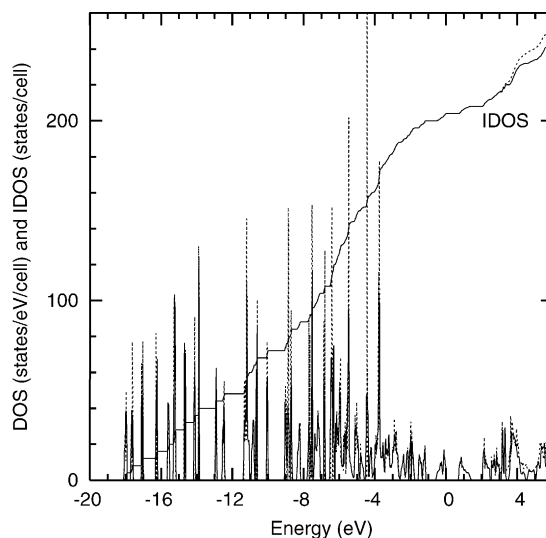

Fig. 2. Density of states in states/eV per cell as function of the energy. The energy is chosen zero at the top of the valence band. Solid line: single crystal, dotted line: cell with the molecules 6 Å apart. Both curves are calculated using a $4 \times 4 \times 2$ mesh. IDOS is the integrated DOS in states (electrons) per cell.

(GGA) [11]. The ab initio total-energy and molecular-dynamics program "Vienna ab initio simulation program" (VASP) was used [12–15]. Electron–ion interactions were described using the projector augmented wave method [16,17]. The kinetic energy cutoff on the wave function expansion was 500 eV.

The self-consistent calculations were carried out using the experimental positions and cell (determination at 90 K from [9]) with a $4 \times 4 \times 2$ *k*-point mesh [18]. Convergence was tested with a $6 \times 6 \times 4$ mesh and found to be sufficient.

The bandstructure of the single molecular layer was calculated also from a three-dimensional crystal, but with an extra vacuum region of 6 Å thickness inserted between the layers. Thus, interactions between the layers were avoided. Moreover, the *c*-axis was chosen perpendicular to the *ab*-plane, i.e. the lattice was transformed to that of a monoclinic crystal.

4. Results

Fig. 2 displays the calculated density of states (DOS) of pentacene. All bands below the Fermi level are completely

filled. The unoccupied bands are separated from the valence bands by a band gap of 0.7 eV. This is consistent with experiment, as undoped pentacene is an insulator. The experimental band gap is 2.2 eV [19]. However, an underestimation of the band gap is not unusual for GGA/DFT and, in general, does not much affect the other features of the electronic structure. The DOS peak of the HOMO (just below 0 eV) and of the LUMO (at 1 eV) are both well separated from the other peaks. Each of them does not mix with bands derived from other molecular states. The calculated HOMO and LUMO bandwidths are ∼600 and 700 meV, respectively. Another, recent theoretical calculation gives values of 608 and 588 meV, respectively [20]. This compares well with our results, although we find a bit wider LUMO band.

Both the DOS of the single layer and of the complete three-dimensional crystal are plotted. On the scale of the plot, differences are only apparent above 3 eV. The electronic structure of the single layer should be a good first approximation to that of the complete crystal. Its bandstructure is only two-dimensional, which greatly facilitates the interpretation.

4.1. Bandstructure of a single layer

The bandstructure near the Fermi level of a molecular layer is depicted in Fig. 3. Both the HOMO and the LUMO complex consist of two bands, as there are two molecules in the unit cell. For both, the maximum and minimum are at *M* $[(1/2, 1/2)]$. Therefore, upon doping (both with electrons and holes) the charge carriers will be created in the vicinity of this point. Their effective mass is strongly directionally dependent. In particular, note the flatness of the bands near
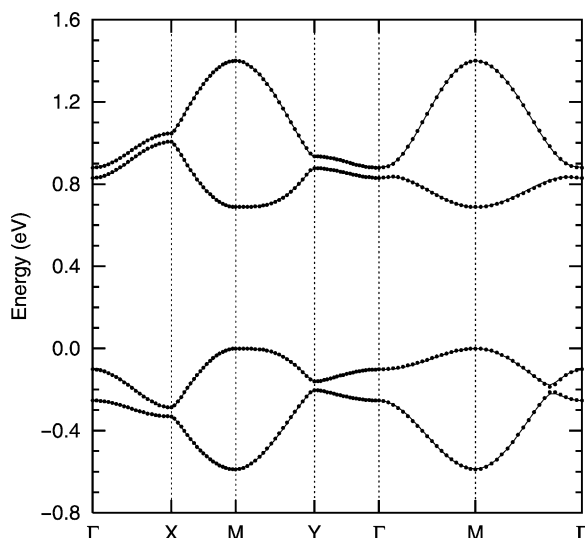
Fig. 3. The bandstructure of one layer of pentacene molecules, with a layer spacing of 6 Å. The energy is chosen to be zero at the top of the valence band. The energies are plotted along lines in the first Brillouin zone, connecting the points $\Gamma = (0,0)$, $X = (\boldsymbol{a}^*/2, 0)$, $M = (\boldsymbol{a}^*/2, \boldsymbol{b}^*/2)$, and $Y = (0, \boldsymbol{b}^*/2)$. From Γ to M is in the direction of $1/2(\boldsymbol{a}^* + \boldsymbol{b}^*)$, from M to Γ is from $1/2(\boldsymbol{a}^* - \boldsymbol{b}^*)$ to Γ. The solid line is the tight binding fit.

Table 1
The following table lists the parameters for the single layer TB fits

	HOMO	LUMO
e (eV)	0.042	0.047
t_a	0.061	−0.041
t_b	−0.004	−0.008
t_{2a}	−0.001	0.000
t_{a+b}	0.003	−0.002
t_{a-b}	0.000	−0.002
$t_{(a+b)/2}$	−0.056	−0.090
$t_{(a-b)/2}$	0.091	0.090
$t_{3(a+b)/2}$	−0.001	0.000
$t_{3(a-b)/2}$	0.001	0.000
$t_{(3a+b)/2}$	0.000	−0.001
$t_{(3a-b)/2}$	0.001	0.001
t_{ae}	0.000	0.003

the extrema for the direction $M-Y$. These observations will be further elaborated upon below.

Since the band complexes are well separated from the other bands, we can attempt a tight-binding fit, for both the HOMO and the LUMO separately. The fit parameters are the transfer integrals t between the molecular orbitals. Some of these are shown in Fig. 4. As we have two molecules, a 2×2 matrix will have to be diagonalized:

$$\begin{bmatrix} \varepsilon(\boldsymbol{k}) - e - T_1 & T_2 \\ T_2 & \varepsilon(\boldsymbol{k}) - T_1 \end{bmatrix} \quad (1)$$

Here, T_1 and T_2 denote the sums of the diagonal and off-diagonal transfer integrals, multiplied with the appropriate phase factors, respectively. $\varepsilon(\boldsymbol{k})$ are the eigenvalues and e accounts for the fact the molecules are inequivalent. $\varepsilon(\boldsymbol{k})$ is
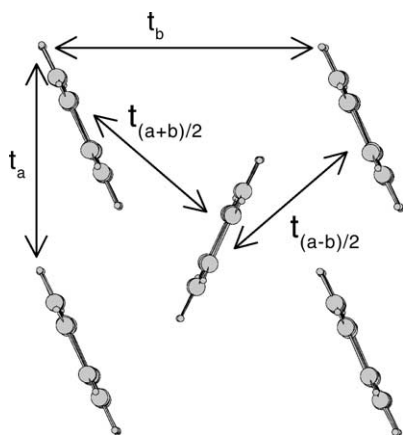
required to follow the DFT result of Fig. 3 as close as possible.

As is evident from the figure, the fit follows the DFT result very well. All transfer integrals are listed in Table 1. By far the most important ones are t_a, $t_{(a+b)/2}$ and $t_{(a-b)/2}$. For the HOMO (LUMO) the values are: $t_a = 31\,(-41)$ meV, $t_{(a+b)/2} = -56\,(-90)$ meV and $t_{(a-b)/2} = 91\,(90)$ meV. All the others are very small.

The effective mass is easily calculated with the help of the analytic expression for the fit. In Fig. 5, the hole effective mass m^*, calculated from

$$-\frac{\partial^2 \varepsilon(\boldsymbol{k})}{\partial k^2} = \frac{\hbar^2}{m^*} \quad (2)$$

is plotted for all directions in the plane. Note the large anisotropy. The largest value, 58 m_e, occurs for the $\boldsymbol{a}$ direction.

Fig. 4. The pentacene $\boldsymbol{ab}$-plane, projected along the long molecular axis. The directions of the different overlap integrals are indicated.
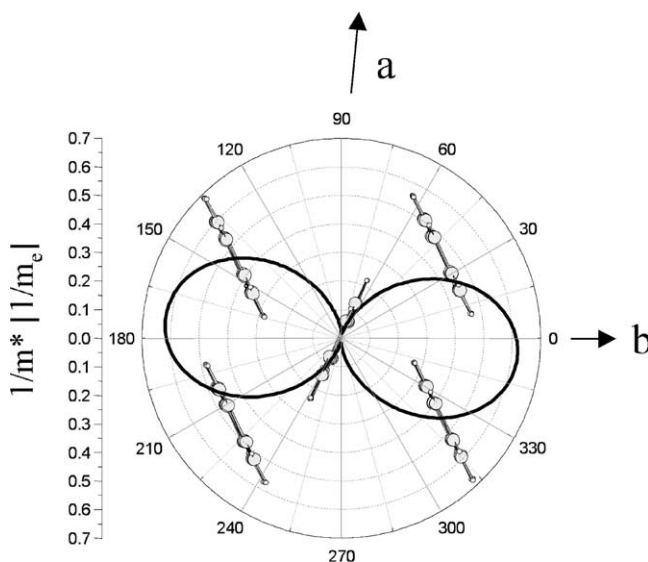

Fig. 5. The reciprocal effective mass as function of the crystallographic direction. Calculations are based on the tight-binding fit of the bandstructure, which is calculated for one layer of pentacene molecules. The pentacene molecules are shown as reference to the crystallographic directions.
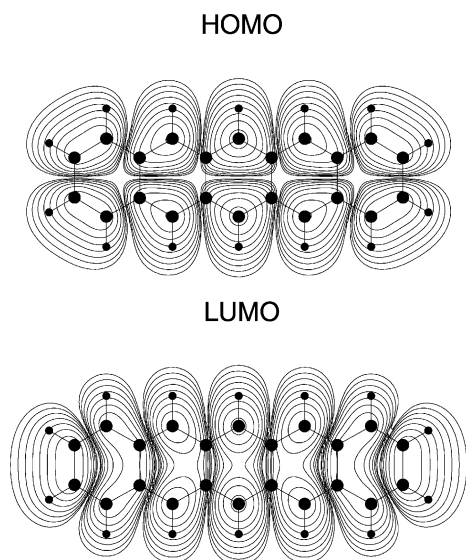
HOMO

LUMO

Fig. 6. Calculated electron densities of the HOMO and the LUMO in a plane above the molecular plane. The large and small black circles indicate the position of the C-atoms and H-atoms, respectively. The lines are on a logarithmic scale. The lines lie at $0.0001 \times 10^{n/3}$ elec/Å^3, $n \geq 1$. The outermost lines have the same electron density.

Below we will further discuss the bandstructure near the M point (i.e. the point where the valence band maximum and conduction band minimum occur) and explain the mechanism behind the large anisotropy. The molecular orbitals, HOMO and LUMO, are plotted in Fig. 6. They are both π-systems, having a nodal plane coinciding with the plane of the molecule. Along the LMA the HOMO alternatingly has maxima and minima that are slightly more apart than the length of one ring-unit of the molecule. This pattern leads to four nodal surfaces "perpendicular" to the LMA. Additionally there is one more nodal plane containing the LMA. The LUMO does not have such a nodal plane. It has two more nodal surfaces "perpendicular" to its LMA. Again the wave function extrema are approximately one ring-unit apart.

Fig. 7 shows a schematic representation, in a plane perpendicular to the LMA, of the HOMO-derived crystal orbitals at the M point. At M the phase of the wave function changes by $180°$, both for a translation over a and b. However, in Fig. 7 all four molecules at the corners have the same phase. This is because the staircase (slant) in the layer gives rise to a shift of the molecule at each step. This results (see the preceding paragraph) in an additional phase change of approximately $180°$.

Depending on the phase of the central molecule, either the low or high band at M is selected. In Fig. 7b, all three important transfer integrals give a bonding contribution. Indeed, this is the most bonding eigenstate within the band complex and thus corresponds to the minimum at M. Fig. 7a depicts the most antibonding situation (the top of the valence band): the transfers $(a + b)/2$ and $(a − b)/2$ are maximally antibonding. Transfer a is still bonding. Due to frustration no
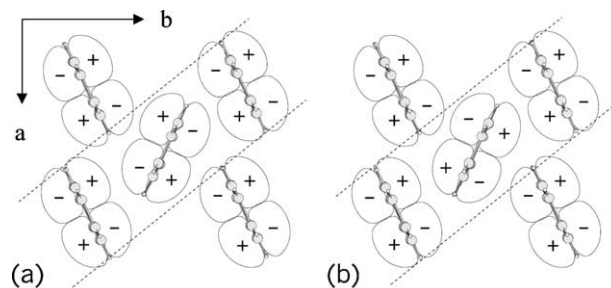

Fig. 7. Crystal orbitals of the HOMO complex at M [(1/2, 1/2)], viewed along the LMA, in a plane perpendicular to the LMA. The HOMO wave functions are schematically depicted with the $+$ and $−$ signs to indicate the phase. (a) The most antibonding situation, as is the case at the top of the valence band. (b) All orbital overlaps are bonding, forming the bottom of the valence band. The dashed lines indicate the shifts between the molecules.

solution with anti-bonding overlap for all three transfers is possible.

The frustration can also explain the large anisotropy in the effective mass. Moving along a ($\approx a^*$) two conduction channels are possible: one directly via t_a, the other via a "double hop" [$t_{(a+b)/2}$ and $t_{(a−b)/2}$]. Moving away from M, the double hop will force the bands in a downward curvature, which is counteracted by the direct channel. This explains why the band becomes flat. By contrast, moving along b^* in reciprocal space, the channel along a drops out and a cosine-shaped band results, indicative of alternate $(a + b)/2$ and $(a − b)/2$ hops.

The LUMO bands mimic the HOMO bands in a very special way: they appear as the "mirror" image of the HOMO bands on the energy axis (Fig. 3). This peculiar feature is due to the LUMO's slightly different nodal structure (it lacks the second mirror plane containing the LMA). Therefore the top point at M has all three transfers antibonding, whereas frustration now occurs for the most bonding point at the bottom of the conduction band (where the a "hop" is still antibonding). Thus the large anisotropy of the hole effective mass is "mirrored" in the electron effective mass. The analogy between the HOMO and LUMO band complex is not complete, e.g. the avoided crossing along $M − \Gamma$ only occurs for the HOMO and the total width of the LUMO complex is slightly larger than that of the HOMO complex.

4.2. Bandstructure of the three-dimensional crystal

The bandstructure of the full three-dimensional crystal (Fig. 8) strongly resembles that of the two-dimensional layer. The shape of the bands for the most dispersive, a^* and b^* directions is essentially the same. Some differences are apparent though: (a) the top of the valence band is not at M [(1/2, 1/2, 0)], but at (0.375, 0.5, 0.075). Moreover, as is evident from the top panel of Fig. 8, the band does not have a parabolic shape. The deviations are small however. The conduction band minimum now occurs near H; (b) a small band dispersion occurs along c^*.
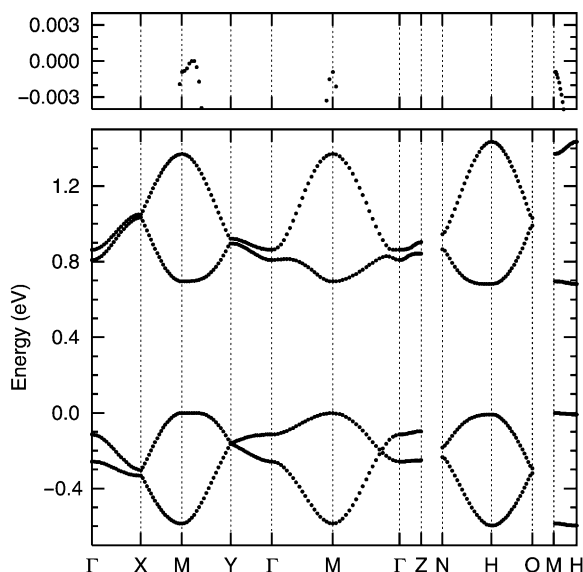
Fig. 8. The bandstructure of single crystalline pentacene. The energy is chosen to be zero at the top of the valence band. The energies are plotted along lines in the first Brillouin zone, connecting the points $\Gamma = (0, 0, 0)$, $X = (a^*/2, 0, 0)$, $M = (a^*/2, b^*/2, 0)$, $Y = (0, b^*/2, 0)$, $Z = (0, 0, c^*/2)$, $N = (0, b^*/2, c^*/2)$, $H = (a^*/2, b^*/2, c^*/2)$ and $O = (a^*/2, 0, c^*/2)$. From Γ to M is in the direction of $1/2(a^* + b^*)$, from M to Γ is from $1/2(a^* - b^*)$ to Γ. The solid line is the tight binding fit. The top graph shows an enlargement of the top of the valence band.

Fig. 9 depicts the hole effective mass, directly calculated from the bandstructure using finite differences. We cannot rely on a TB fit, as it cannot capture the bump at (0.375, 0.5, 0.075). For directions close to a^* the effective mass was not calculated, due to the locally non-parabolic nature of the band. For the other directions the picture is very similar
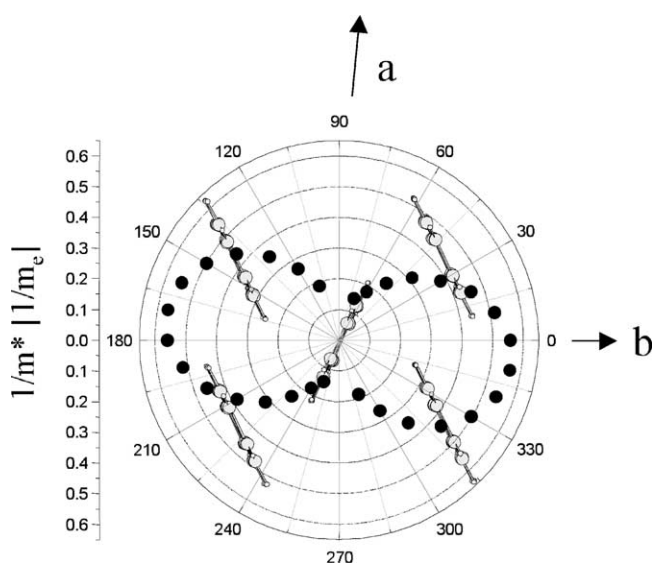

Fig. 9. The reciprocal effective mass as function of the crystallographic direction. Calculations are based on the bandstructure of single crystalline pentacene. The pentacene molecules are shown as reference to the crystallographic directions.

to the two-dimensional analogon. For c^*, we obtain: $m_{c^*}^* = 5.2\, m_e$.

Our results may be compared with a recent extended Hückel (EH) bandstructure calculation on the pentacene single crystal [21]. The agreement between the EH and our first-principles results is quite good. The EH study reports the bandstructure for a limited number of lines in the BZ (Γ–X, Γ–Y, Γ–Z) and therefore does not consider the special situation near M.

5. Discussion and conclusions

Bandstructure calculations for the pentacene single crystal reveal HOMO and LUMO bandwidths of ∼600 and 700 meV, respectively. Consistently, (hole) effective masses as low as $1.7 m_e$ (for m_{b^*}) are found. Even $m_{c^*}^*$ ($5.2 m_e$) is rather low, in spite of the apparent flatness of the bands for the c^* direction. Within the molecular layers, a competition between different conduction paths results in a large anisotropy of both the hole and the electron effective mass, the charge carriers being orders of magnitude heavier for the a^* (than for the b^* direction).

Our calculations do not take into account the coupling with lattice degrees of freedom. At lower temperatures the electron–phonon coupling may renormalize the charge carrier's bandwidth. At higher temperatures the bandwidth renormalization and mobility reduction may differ for different directions, thus affecting the anisotropy. For anthracene, recent first-principles calculations indeed show a directionally dependent bandwidth renormalization [22]. However, as it is so pronounced, we expect much of the effective mass anisotropy to survive, also at higher temperatures, as long as coherent band-like transport is dominant.

References

[1] S.F. Nelson, Y.-Y. Lin, D.J. Grundlach, T.N. Jackson, Appl. Phys. Lett. 72 (1998) 1854.

[2] Y.-Y. Lin, D.J. Grundlach, S.F. Nelson, T.N. Jackson, IEEE Trans. Electr. Dev. 44 (1997) 1325.

[3] W. Warta, N. Karl, Phys. Rev. B 32 (1985) 1172.

[4] R.C. Haddon, A.S. Perel, R.C. Morris, T.T.M. Palstra, A.F. Hebard, R.M. Fleming, Appl. Phys. Lett. 67 (1995) 121.

[5] R.A. Laudise, C. Kloc, P. Simpkins, T. Siegrist, J. Cryst. Growth 187 (1998) 449.

[6] C.C. Mattheus, J. Baas, A. Meetsma, J.L. de Boer, C. Kloc, T. Siegrist, T.T.M. Palstra, Acta Cryst. E 58 (2002) o1229 .

[7] C.C. Mattheus, A.B. Dros, J. Baas, G.T. Oostergetel, A. Meetsma, J.L. de Boer, T.T.M. Palstra, Synth. Met., in press.

[8] D. Holmes, S. Kumaraswamy, A.J. Matzger, K.P.C. Vollhardt, Chem. Eur. J. 5 (1999) 3399.

[9] C.C. Mattheus, A.B. Dros, J. Baas, A. Meetsma, J.L. de Boer, T.T.M. Palstra, Acta Cryst. C 57 (2001) 939.

[10] T. Siegrist, Ch. Kloc, J.H. Schön, B. Batlogg, R.C. Haddon, S. Berg, G.A. Thomas, Chem. Angew. Int. Ed. 40 (2001) 1732.

[11] J.P. Perdew, J.A. Chevary, S.H. Vosko, K.A. Jackson, M.R. Pederson, D.J. Singh, C. Fiolhais, Phys. Rev. B 46 (1992) 6671.

[12] G. Kresse, J. Hafner, Phys. Rev. B 47 (1993) 558.

[13] G. Kresse, J. Hafner, Phys. Rev. B 49 (1994) 14251.

[14] G. Kresse, J. Furthmüller, Comput. Mater. Sci. 6 (1996) 15.

[15] G. Kresse, J. Furthmüller, Phys. Rev. B 54 (1996) 11169.

[16] P.E. Blöchl, Phys. Rev. B 50 (1994) 17953.

[17] G. Kresse, D. Joubert, Phys. Rev. B 59 (1999) 1758.

[18] H.J. Monkhorst, J.D. Pack, Phys. Rev. B 13 (1976) 5188.

[19] E.A. Silinsh, Organic Molecular Crystals, Springer, Berlin, 1980.

[20] J. Cornil, D. Beljonne, J.-P. Calbert, J.-L. Brédas, Adv. Mat. 13 (2001) 1053;
J. Cornil, J.-P. Calbert, J.-L. Brédas, J. Am. Chem. Soc. 123 (2001) 1250.

[21] R.C. Haddon, X. Chi, M.E. Itkis, J.E. Anthony, D.L. Eaton, T. Siegrist, C.C. Mattheus, T.T.M. Palstra, J. Phys. Chem. B 106 (2002) 8288.

[22] K. Hannewald, V.M. Stojanović, J.M.T. Schellekens, P.A. Bobbert, G. Kresse, J. Hafner, submitted for publication.